Passively Q-switched single-frequency output from a diffusion-bonded monolithic Nd:YAG non-planar ring oscillator

Mingwei Gao (高明伟)*, Fuyong Yue (岳夫永), Tie Feng (冯 铁), Jialong Li (李佳龙), and Chunqing Gao (高春清)

School of Opto-Electronics, Beijing Institute of Technology, Beijing 100081, China

**Corresponding author: ghew@bit.edu.cn*

Received October 25, 2013; accepted December 23, 2013; posted online January 24, 2014

A compact monolithic Nd:YAG non-planar ring laser with diffusion-bonded Cr^{4+}:YAG is demonstrated, and high stable pulsed single-frequency laser at 1.06 μm is realized. Theoretical analysis and simulation results of pulsed laser parameters are illustrated. 14.96-kW maximum peak power, pulse-width of 4.8 ns is achieved for single-frequency operation.

OCIS codes: 140.3540, 140.3560, 140.3570.
doi: 10.3788/COL201412.021404.

Pulsed single-frequency lasers have many potential applications in such areas as coherent lidars, micromachine, metrology, and coherent imaging[1,2]. Passive Q-switching as a simple and effective approach for achieving pulsed output has been widely reported[3−5]. While, the pulse energy of passively Q-switching lasers using the conventional standing-wave cavity is unstable because of spatial hole burning. Monolithic non-planar ring oscillator (NPRO), firstly developed by Kane *et al.*[6], has been widely documented due to its advantage of high stability single frequency operation, narrow linewidth and low frequency noises[7−9]. In 1995, Braun *et al.* demonstrated Q-switched operation of NPRO by using Fabry-Perot saturable absorbers[10]. However, the low peak power (a few Watts) and the cost limited its applications. In 1997, Freitag *et al.* reported passively Q-switched single frequency Nd:YAG ring laser by using Cr^{4+}:YAG[11]. Although it realized peak power of 30 kW, energies of 70-μJ output, the construction was discrete. And the faces of Nd:YAG near the saturable absorber should be antireflection coated to minimize the transmission loss.

In this letter, we demonstrate a diode pumped monolithic Nd:YAG (NPRO) with a diffusion-bonded saturable absorber Cr^{4+}:YAG. The stability of the oscillator was ensured by bonding the saturable absorber to the gain medium. The schematic draw of the monolithic double diffusion-bonded Nd:YAG NPRO crystal is shown in Fig. 1. The first parts is undoped YAG to reduce the residual spatial hole burning and thermal effect[12,13]. The second crystal segment is the Cr^{4+}:YAG which is used as saturable absorbers to ensure passively Q-switched operation. The third parts is the active Nd:YAG gain media for the laser process with 1.0 at.-% doping concentration. The facets containing B, C, and D are optically polished flat surfaces on the Nd:YAG crystal where total internal reflections occur. The front surface A is dielectrically coated for high transmission at the pump wavelength of 808 nm and a few percent output coupling at the laser wavelength. Stable single-frequency operation is accomplished by enforcement of unidirectional operation owing to an intrinsic optical diode. To achieve the optical diode we applied a permanent magnetic field of ∼0.25 T along the crystal. The unidirectional laser oscillation of NPRO cavity will significantly reduce the fluctuation of output pulse energy of passively Q-switched Cr^{4+}:YAG laser. The combination of NPRO cavity and Cr^{4+}:YAG ensure a stable single frequency Q-switched laser oscillation.

The dynamics of the Q-switched process could be simulated with the help of rate equations. The relevant rate equations for passively Q-switched lasers were firstly derived by Szabo *et al.*[14]. Degnan optimized and simplified the equations by employing several rational approximations and analytically calculated the parameters of pulsed laser[15]. The pulse energy and pulse peak power can be given by

$$E_{\mathrm{p}} = \frac{hvA}{2\sigma\gamma} \ln\left(\frac{1}{R}\right) \ln\left(\frac{n_i}{n_f}\right), \tag{1}$$

$$P_{\mathrm{peak}} = \frac{hvA \ln(\frac{1}{R})c}{2} n_i \Big\{1 - \frac{n_t}{n_i} + N \ln\Big(\frac{n_t}{n_i} - \frac{1}{\alpha}(1-N) \Big[1 - \Big(\frac{n_t}{n_i}\Big)^{\alpha}\Big]\Big)\Big\}, \tag{2}$$

where A is the effective beam area, h is Planck's constant, v is the laser frequency, R is the reflectivity of output coupler, c is the speed of light, σ is the laser emission

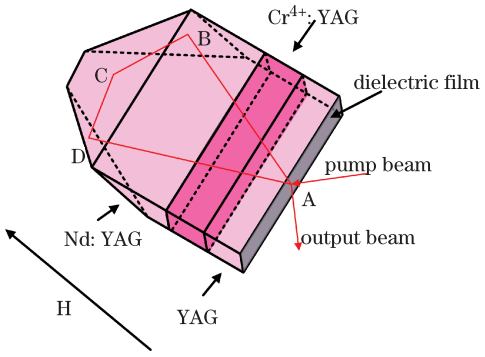

Fig. 1. Schematic of Nd:YAG NPRO with diffusion-bonded Cr^{4+}:YAG.

cross section, γ is population reduction factor, which equals 1 for an ideal four-level laser, α is a special parameter of passively Q-switched laser. The larger α indicates more easily bleached of the saturable absorber. n_i, n_t, and n_f are the initial population inversion density at the start of Q-switching, the inversion density at the point of maximum power, and the final inversion density respectively. They are given by

$$n_i = \frac{\ln(\frac{1}{T_0^2}) + \delta}{2\sigma l}, \tag{3}$$

$$\frac{n_t}{n_i} = N + (1-N)\left(\frac{n_t}{n_i}\right)^{\alpha}, \tag{4}$$

$$\frac{n_f}{n_i} = 1 + N\ln\left(\frac{n_f}{n_i}\right) - \frac{1}{\alpha}\left[1 - \left(\frac{n_f}{n_i}\right)^{\alpha}\right], \tag{5}$$

where $\delta = \ln(\frac{1}{R}) + L$ is the total loss of cavity, l is the length of gain medium. N is defined as $N = \frac{\beta\ln(\frac{1}{T_0^2})+\delta}{\ln(\frac{1}{T_0^2})+\delta}$. Note that $\beta = \frac{\sigma_{2s}}{\sigma_{1s}} = \frac{\ln T_s}{\ln T_0}$. σ_{1s} and σ_{2s} are the saturable absorber (SA) absorption cross section of ground-state, and stimulated-state respectively. T_s and T_0 are saturable transmission and initial transmission of saturable absorbers respectively. The pulse width and repetition rate can be obtained as

$$t_p \approx \frac{E_p}{P_{peak}}, \tag{6}$$

$$f = \frac{1}{\tau_a}\frac{\frac{R}{R_{th}} - (1+\frac{1}{\beta})/2}{1-\frac{1}{\beta}}, \tag{7}$$

where τ_a is the lifetime of the upper level of the gain medium, R and R_{th} are the pump rate and threshold pump rate respectively, $\beta = 1 - \frac{f_a}{\gamma}(1-\frac{n_f}{n_i})$, f_a is the Boltzmann occupancy factor for the stark level. It is clear that all the parameters of pulse are as a function of inversion densities n_i, n_t, and n_f. And all the inversion densities depend on two important coefficients T_0 and R. Figure 2 illustrates the parameters of pulse as a function of R at different initial transmissions T_0 of 60%, 70%, 80%, and 90%.

From Fig. 2(a), it can be seen that peak power of pulsed laser decreases with increasing reflectivity R from 0.7 to 1. For a given reflectivity R, higher initial transmission T_0 leads to lower peak power. Figure 2(b) plots pulse width as a function of R at different T_0 (60%, 70%, 80% and 90%). When T_0 is 90%, pulse width initially decreases and then increases slightly with increasing R. When T_0 is at 60%, 70% and 80%, they all experience little rise with R. Higher T_0 leads to larger pulse width. Pulse energy experiences the similar trend with peak power (see Fig. 2(c)). Lower T_0 and R lead to higher pulse energy. Figure 2(d) shows that repetition rate increases with both T_0 and R. The simulation results of pulse parameters guide the optimization of laser design. If one need higher peak power laser with low repetition rate and shorter pulse, saturable absorbers with lower T_0 combined with lower reflectivity of output coupler should be chosen. On the contrary, when needing high repetition rate pulsed laser with lower pulse energy, saturable absorbers with higher T_0 should be used.

The experimental setup of the monolithic Nd:YAG NPRO with diffusion-bonded Cr^{4+}:YAG pumped by a 808-nm laser diode is illustrated in Fig. 3. The geometrical size of the diffusion bonded crystal was 12×9.8×4 (mm). The width of the saturable absorber was 2 mm. The width of the undoped YAG was also set 2 mm to minimize the thermal effect. The Nd-doping concentration of the gain medium was 1.1 at.-%. According to the simulation results, the Cr-doping concentration of the saturable absorber was chosen for the initial transmission T_0 of 80%. The input surface (also was output coupler) was multi-dielectric coated for a high transmission at 808 nm and for a 15% output coupling of the s-polarized beam at 1.06 μm. The pump beam was focused into the monolithic NPRO by a 1:1 coupling optics.

In Fig. 4, the dependencies of the pulse parameters on the pump power are shown. The average output power and pulse frequency exhibited an approximate linear dependence on the pump power increased from ~5.5 to 10 W. In single-frequency operation, the maximum average output power was 466 mW with the slope efficiency of 26.8%. The peak power exhibited a non-linear increase on the pump power, with a simultaneous shortening of the pulse width.

To confirm single frequency operation of the pulsed laser, the output beam was coupled into a Fabry-Peort cavity. A charge-coupled device (CCD) camera was used

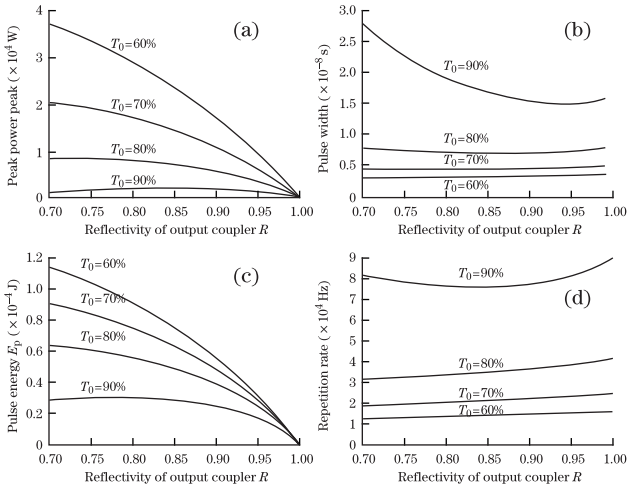

Fig. 2. (a) Peak power, (b) pulse width, (c) pulse energy, and (d) repetition rate versus reflectivity of output coupler R for different T_0 with a pump power of 5 W.

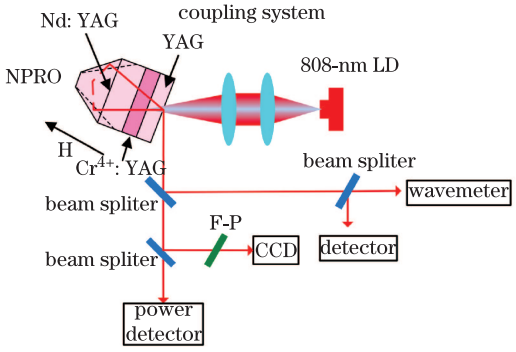

Fig. 3. Experimental schematic diagram of Nd:YAG NPRO with diffusion-bonded Cr^{4+}:YAG pumped by a laser diode.

to monitor the interfered laser beam. Figure 5 shows the interference fringe of output beam with magnetic field and without magnetic field. It is clear that only one set of fine fringe observed in (Fig. 5(a)), whereas (Fig. 5(b)) has two sets of fringe which meant that the laser was under multi-mode operation.

The stability of the output pulse train was investigated using an oscilloscope (Tektronix TDS5052B). Figure 6 shows the envelope of pulse with 10000 times accumulation and pulse train with 1000 times accumulation. It confirmed the stability of pulse energy of the Q-switched single-frequency ring laser. The beam quality of laser beam was measured at the maximum output power in single-frequency operation. Figure 7 illustrates the measured beam radii at different positions. M^2 factors were calculated to be 1.35 and 1.4 in the x direction and y direction, respectively, by fitting the data with a hyperbolic curve. For this configuration approximately 7% of pump energy was absorbed by Cr^{4+}:YAG after reached the gain medium. The initial transmission of saturable absorber would be higher than 80% because part of ground-state population was excited to the upper level. This effect leads to higher threshold (~5.88 W) and lower pulse energy.

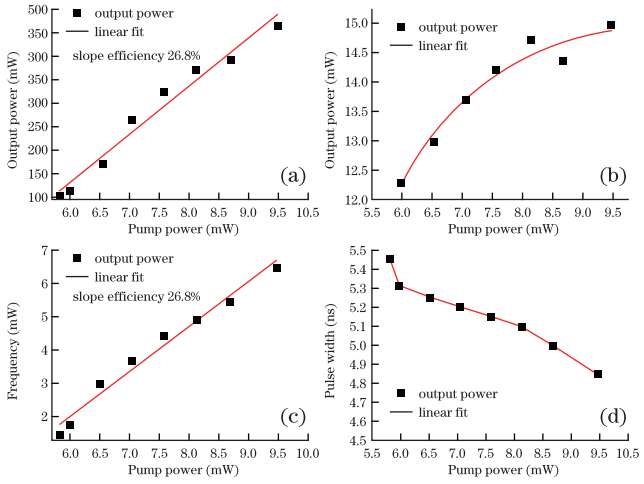

Fig. 4. Output average power, peak power, repetition rate, and pulse width versus optical pump power.

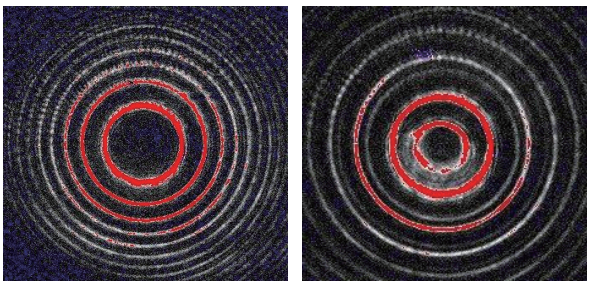

(a) (b)

Fig. 5. Interference fringe of output beam (a) with and (b) without magnetic field.

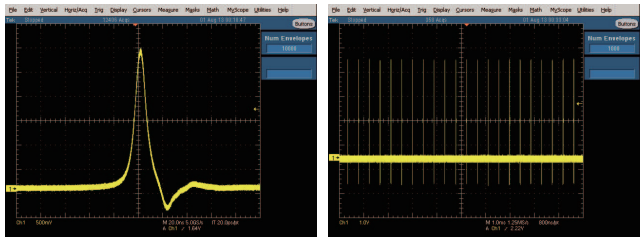

(a) (b)

Fig. 6. Envelope of pulses and pulse train.

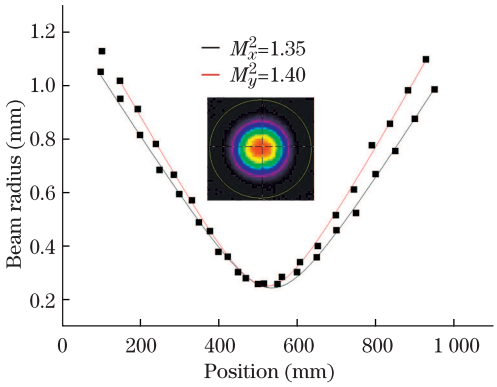

Fig. 7. M^2 factor calculated by nonlinear fitting and beam profiles of the pulsed single-frequency NPRO with diffusion-bonded Cr^{4+}:YAG.

In conclusion, we demonstrate a pulsed single-frequency operation in diode pumped monolithic NPRO at 1.06 μm. The undoped YAG eliminates the residual spatial hole burning under high power pump condition. Average output power of 466 mW and pulse energy of 70.08 μJ are generated. The maximum pulse peak power is 14.96 kW. 4.8-ns-long (FWHM) pulses at a repetition rate of 6.49 kHz are observed. The simple and compact passively Q-switched laser design makes it as an ideal coherent light source for applications of coherent lidar, coherent imaging, and other fields which require pulse and single-mode operation.

References

1. J. Yun, C. Gao, S. Zhu, C. Sun, H. He, L. Feng, L. Dong, and L. Niu, Chin. Opt. Lett. **10,** 121402 (2012).
2. X. Zhu, J. Liu, D. Bi, J. Zhou, W. Diao, and W. Chen, Chin. Opt. Lett. **10,** 012801 (2012)
3. M. Laroche, A. M. Chardon, J. Nilsson, D. P. Shepherd, and W. A. Clarkson, Opt. Lett. **27,** 1980 (2002).
4. L. Pan, I. Utkin, and R. Fedosejevs, IEEE J. Photon. Technol. Lett. **19,** 1979 (2007).
5. G. J. Spühler, R. Paschotta, M. P. Kullberg, M. Graf, M. Moser, E. Mix, G. Huber, C. Harder, and U. Keller, Appl. Phys. B. **72,** 285 (2001).
6. T. J. Kane and R. L. Byer, Opt. Lett. **10,** 65 (1985).
7. P. Burdack, T. Fox, M. Bode, and I. Freitag, Opt. Express. **14,** 4363 (2006).
8. C. Gao, M. Gao, Y. Zhang, Z. Lin, and L. Zhu, Opt. Lett. **34,** 3029 (2009).
9. B. Q. Yao, X. Yu, X. L. Liu, X. M. Duan, Y. L. Ju, and Y. Z. Wang, Opt. Express **21,** 8916 (2013).

10. B. Braun and U. Keller, Opt. Lett. **20,** 1020 (1995)
11. I. Freitag, A. Tünnermann, and H. Welling, Opt. Lett. **22,** 706 (1997)
12. K. I. Martin, W. A. Clarkson, and D. C. Hanna, Opt. Commun. **125,** 359 (1996).
13. M. Gao, Y. Zhao, L. Zhang, L. Wang, and C. Gao, Chin. Opt. Lett. **11,** 041406 (2013).
14. A. Szabo and R. A. Stein, J. Appl. Phys. **36,** 1562 (1956).
15. J. J. Degnan, IEEE J. Quantum Electron. **31**, 1890 (1995).